

# Multiple RIS-Assisted Mixed FSO-RF Transmission Over Generalized Fading Channels

Vinay Kumar Chapala, *Graduate Student Member, IEEE* and S. M. Zafaruddin, *Senior Member, IEEE*

**Abstract**—In this paper, we analyze the performance of a reconfigurable intelligent surface (RIS)-assisted multi-hop transmission by employing multiple RIS units to enable favorable communication for a mixed free-space optical (FSO) and radio-frequency (RF) system. We consider a single-element RIS since it is hard to realize phase compensation for multiple-element RIS in the multi-hop scenario. We develop statistical results for the product of the signal-to-noise ratio (SNR) of the cascaded multiple RIS-equipped wireless communication. We use decode-and-forward (DF) and fixed-gain (FG) relaying protocols to mix multi-RIS transmissions over RF and FSO technologies and derive probability density and distribution functions for both the relaying schemes by considering independent and non-identical double generalized gamma (dGG) distribution models for RF transmissions with line-of-sight (LOS) and inverse-Gamma shadowing effect and atmospheric turbulence for FSO system combined with pointing errors. We analyze the outage probability, and average bit-error rate (BER) performance of the considered system. We also present an asymptotic analysis of the outage probability using gamma functions to provide insight into the considered system in the high SNR regime. We use computer simulations to validate the derived analytical expressions and demonstrate the performance for different system parameters on the RIS-assisted multi-hop transmissions for a vehicular communication system.

**Index Terms**—Multiple RIS, performance analysis, reconfigurable intelligent surface, relaying, vehicular communications.

## I. INTRODUCTION

Traditionally, wireless communication systems are optimized based on the principle that channel environments cannot be configured. Adaptive modulation, optimization of transmit power, diversity techniques, and cooperative relaying are methods to mitigate channel impairments such as channel fading, path loss, and shadowing effect. It is intriguing to accept that signal propagation in an unknown environment due to scattering, reflection, and refraction of electromagnetic waves can be controlled. Reconfigurable intelligent surface (RIS) is evolving as a next-generation technology for reliable wireless and vehicular communications [2]–[5]. In general, RIS modules consist planar structures of metasurfaces that can be intelligently programmed to steer the incident waves in a particular direction. An RIS unit accommodating many meta elements to reflect the signal is being considered a potential alternative to cooperative relaying for 6G wireless systems. In recent years, free-space optical (FSO) for backhaul/fronthaul

and radio frequency (RF) for broadband access have been considered as a potential architecture for next generation wireless communications [6]. The FSO is potential technology with a higher contiguous unlicensed optical spectrum, which can be employed for secured high data rate transmissions for backhaul applications. The RIS can help FSO and RF links to maintain line-of-sight (LOS) connectivity for an improved performance for both vehicular and terrestrial communications.

Recent research focus on the applicability of a single RIS (mostly with multiple elements) based wireless systems for intelligent vehicular communications [7], [8], low-frequency radio-frequency (RF) [9], [10], optical wireless communications (OWC) [11]–[14], and high-frequency terahertz (THz) wireless systems [15]–[17]. However, the use of multiple RIS module can provide reliable connectivity for different situations. Ozcan *et al.* in [18] provided optimized algorithms for placing multiple RISs alongside the road for vehicle-to-everything (V2X) infrastructure. Huang *et al.* [19] suggested hybrid beamforming under multi-hop scenario to extend the transmission range at terahertz frequencies. Boulogeorgos *et al.* [20] analyzed the performance of a cascaded FSO system assisted by multiple RIS modules (with single-element) considering Gamma-Gamma atmospheric turbulence and pointing errors. They applied the method of induction to derive the probability density function (PDF) and cumulative distribution function (CDF). It is known that the double generalized Gamma (dGG) distribution for the atmospheric turbulence in FSO system is superior to the Gamma-Gamma model since the dGG model is valid under all range of turbulence conditions (weak to strong) for both plane and spherical waves propagation [21]–[24]. Further, the dGG model is an appropriate model for radio propagation for V2V communications over RF frequencies [25]. The dGG is a generalized model consisting most of the existing statistical models as particular cases. To this end, it should be mentioned that the induction method of [20] may not be applicable for the cascaded dGG fading model to conduct performance analysis for wireless transmission empowered by multiple RIS units.

There has been some study on the performance of a single RIS (equipped with multiple elements) assisted mixed FSO-RF systems [26]–[29]. In [26]–[28], the authors used the near-optimal decode-and-forward (DF) relaying protocol to integrate an FSO transmission link and RIS-equipped RF link distributed according to the simpler Rayleigh fading model. In [28], authors analyzed the performance of a RIS-equipped source mixed RF/FSO system by considering RIS located close to the source in the RF link. It should be mentioned that fixed-gain amplify-and-forward (AF) relaying is well acknowledged for its desirable characteristics of lower computational complexity and the fact that it does not require continuous channel monitoring for decoding at the relay [30]. Further, deriving analytical results for fixed-gain AF relaying with general channel models is challenging compared with the

This work was supported in part by the Science and Engineering Research Board (SERB), Government of India, under MATRICS Grant MTR/2021/000890.

A conference version of the paper analyzing the RF link consisting of multiple RIS over dGG fading was presented at the 2022 IEEE 95th Vehicular Technology Conference (VTC 2022-Spring), Helsinki, Finland, 19-22 June 2022 [1].

The authors are with the Department of Electrical and Electronics Engineering, Birla Institute of Technology and Science, Pilani, Pilani-333031, Rajasthan, India, Email: p20200110@pilani.bits-pilani.ac.in, syed.zafaruddin@pilani.bits-pilani.ac.in.

DF protocol. The authors in [29] investigated the outage probability performance of a fixed-gain relayed system for the mixed RF-visible light communication for an indoor environment. To the best of authors' knowledge, a multiple RIS empowered mixed FSO-RF relayed system over dGG fading channels has not been reported in the literature.

This paper analyzes the performance of a mixed FSO-RF system by employing multiple RISs in both the links realizing multi-hop transmissions for reliable connectivity. We assume the dGG turbulence model and zero-boresight pointing errors for the FSO link and the dGG distribution to model the signal fading combined with the effect of shadowing distributed as inverse-Gamma (IG) for vehicular transmissions over RF along with the LOS link and a statistical model for mobility. The major contributions of the paper are listed as follows:

- We consider a single-element RIS since it is hard for phase compensation to be realized for multiple-element RIS in a multi-hop scenario.
- We develop statistical results for the product of the signal-to-noise ratio (SNR) of the cascaded multiple RIS-equipped wireless communication.
- We derive PDF and CDF of the fixed-gain (FG) relaying using Fox's H-function to mix multi-RIS empowered vehicular transmissions over RF and FSO backhaul with zero-boresight pointing errors considering independent and non-identical (i.n.i.d) double generalized gamma (dGG) distribution function without any constraint on its fading parameters.
- We analyze the performance of the AF-assisted system by deriving exact analytical expressions of the outage probability and average bit-error-rate (BER) in terms of trivariate Fox's H-function. We also analyze the performance by integrating the FSO and RF systems using the DF relaying in terms of bivariate Fox's H-function.
- We present asymptotic analysis of the outage probability in terms of simpler Gamma functions to develop better insight on the system performance in the high SNR regime.

## II. DESCRIPTION OF THE SYSTEM MODEL

Consider a multi-hop mixed FSO/RF system assisted by multiple RISs in both FSO and RF links, as depicted in Fig. 1. The source ( $S$ ) desires to connect with a moving vehicle ( $V$ ). We consider a communication link comprising of backhaul/fronthaul on the FSO technology and vehicular link on the RF. A relay ( $R$ ) with the functionality of AF/DF is deployed to integrate the FSO and RF technologies. The relay contains a photodetector for receiving FSO signals and a frequency down-converter for low frequency RF communications. We employ multiple optical RIS to assist the communication from the source to the relay over a building-to-building backhaul link since there is no direct link between them for the line-of-sight FSO transmissions. In FSO links, the use of multiple RIS modules may reduce the pointing error in each hop due to near-perfect beam alignment with subsequent use of multiple RIS. Thus, the source communicates data to the relay through  $K_1$  hops using  $K_1 - 1$  optical RIS modules. Further, we employ  $K_2 - 1$  RF RIS modules perpendicular to the road such that the desired vehicle is connected to any one of the RIS modules. With the multiple RF-RIS deployment, the effect of deep shadowing can be reduced due to the close proximity of the moving vehicle to RIS.

We assume that each optical RIS reflects the incident beam towards subsequent optical RIS until the last RIS directs the beam towards the relay. We assume perfect knowledge of the

channel at each RIS to perform phase control. Indeed, practical algorithms are needed to estimate the channel at each RIS to better reflect the incident signal in a desired direction. In a recent paper [31], a different system configuration has been considered by employing multiple RIS such that the destination directly receives signals from each RIS independent of other RIS. We consider single-element RIS in the multi-hop situation as phase compensation in a multiple-element RIS under a multihop deployment scenario is hard to realize. Thus, the signal  $y_R$  at the relay unit through  $(K_1 - 1)$  optical RISs is given by

$$y_R = \prod_{i=1}^{K_1} h_i A_i^{FSO} e^{j\theta_i^{FSO}} s + w_R \quad (1)$$

where  $h_1$  denotes the channel coefficient from the transmission source to the first-optical RIS whereas  $h_i$  is the channel coefficient from  $(i - 1)$ -th optical RIS to  $i$ -optical RIS. Here,  $h_{K_1}$  is the channel coefficient of the last  $(K_1 - 1)$ -optical RIS to the relay.  $s$  is the transmitted signal with power  $P$ , and  $w_R$  is the additive white Gaussian noise (AWGN) with variance  $\sigma_R^2$ . The terms  $A_i$  and  $\theta_i^{FSO}$  denote the gain and phase of the  $i$ -th FSO-RIS module, respectively.

Similarly, the signal at destination vehicle connected through  $(K_2 - 1)$ -th RIS along with LOS signal is given by

$$y = \prod_{i=1}^{K_2} g_i A_i^{RF} e^{j\theta_i^{RF}} s + g_{LOS} s + w_V \quad (2)$$

where  $w_V$  is the AWGN at the destination with noise variance  $\sigma_V^2$ ,  $g_1$  is the channel coefficient from the relay to the first RIS,  $g_i$  is the channel from  $(i - 1)$ -th RIS to  $i$ -RIS, and  $g_{K_2}$  is the channel coefficient of the last  $(K_2 - 1)$ -RIS to destination vehicle. The terms  $A_i^{RF}$  and  $\theta_i^{RF}$  denote the gain and phase of the  $i$ -th RF-RIS module, respectively. Here,  $g_{LOS}$  is the channel coefficient of LOS link from the relay to destination vehicle.

We consider the dGG distribution to model the atmospheric turbulence for the FSO and as multi-path fading model for the RF link. As such, the dGG is the product of two generalized Gamma functions. The PDF of the generalized Gamma function is given as

$$f_X(x) = \frac{\alpha x^{\alpha\beta-1}}{(\frac{\Omega}{\beta})^\beta \Gamma(\beta)} \exp(-\frac{\beta}{\Omega} x^\alpha) \quad (3)$$

where  $\alpha, \beta$  are shaping parameters of the Gamma distribution and  $\Omega = (\frac{\mathbb{E}[X^2] \Gamma(\beta)}{\Gamma(\beta+2/\alpha)})^{\alpha/2}$  is the  $\alpha$ -root mean value parameter.

In addition to the atmospheric turbulence, we include pointing errors in each hop of the FSO link such that the resultant channel becomes  $h_i = h_i^{(l)} h_i^{(t)} h_i^{(p)}$ , where subscripts  $(l)$ ,  $(t)$  and  $(p)$  denote path gain, atmospheric turbulence coefficient and pointing error coefficient. To characterize pointing errors statistically, we use the recent model proposed in [32]:

$$f_{h_i^{(p)}}(x) = \frac{\rho_i^2}{A_{0,i} \rho_i^2} x^{\rho_i^2-1}, 0 \leq x \leq A_{0,i}, \quad (4)$$

where the term  $A_{0,i}$  denotes the fraction of collected power at the receiver aperture and  $\rho_i^2 = \frac{\omega_{zeq}^2}{\xi}$  where  $\omega_{zeq}$  is the equivalent beam-width at the receiver. The lower value of  $\rho_i$  and  $A_{0,i}$  indicates higher pointing error. An extension to the non-zero boresight pointing errors is also possible, however, with more complicated analytical derivations [33].

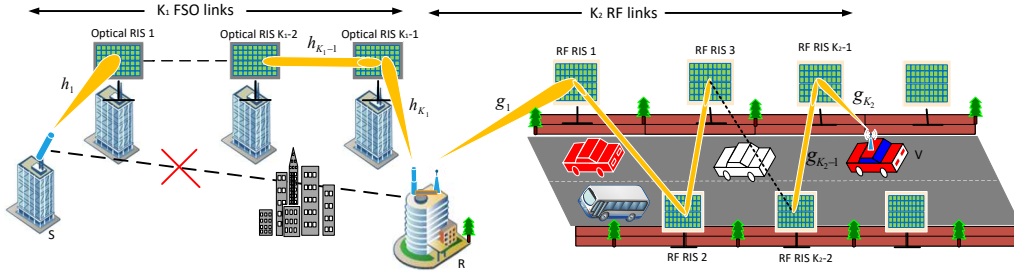


Fig. 1. A block diagram description for multiple RIS empowered vehicular communications.

Similarly, we denote the channel coefficient between the  $(i-1)$ -th and  $i$ -th RIS as  $g_i = g_i^{(l)} g_i^{(s)} g_i^{(f)}$ , where subscripts  $(l)$ ,  $(s)$  and  $(f)$  denote path loss, shadowing and short-term fading coefficients of RF links. Moreover, we include the analysis of direct link represented as  $g_{\text{LOS}} = g_{\text{LOS}}^{(l)} g_{\text{LOS}}^{(s)} g_{\text{LOS}}^{(f)}$ . Note that many models exist in the literature to characterize the effect of shadowing. However, we use more recently proposed IG model which is validated through practical measurements and analytical tractability. We consider the IG distribution to model the effect of shadowing whose PDF is obtained using [34, eq. 5] and through transformation of random variables, we get

$$f_{g_i^{(s)}}(x) = \frac{2(m_i - 1)}{\Gamma(m_i)} x^{2m_i - 1} \exp\left(-\frac{m_i - 1}{x^2}\right) \quad (5)$$

The path loss component of each RF link is considered as  $g_i^{(l)} = \left(\frac{c}{4\pi f_c d_{K_2}}\right)^2$ , where  $d_{K_2}$  is the length of each hop,  $c = 3 \times 10^8$  m/s, and  $f_c$  is the center frequency. Note that the path-loss  $g_{K_2}^{(l)}$  between the RIS and destination vehicle is random considering the movement of the vehicle. We denote that path loss component of last hop as  $g_{K_2}^{(l)} = r^{-\frac{a}{2}}$ , where  $a, 2 \leq a \leq 5$  is the path loss exponent factor. We assume random way point (RWP) mobility model for the path loss with probabilistic distance  $r$  of the last hop,  $0 \leq r \leq d_{K_2}$  [35]:

$$f_r(x) = 6 \frac{x}{d_{K_2}^2} - 6 \frac{x^2}{d_{K_2}^3} \quad (6)$$

It should be mentioned that the received signal in (1) and (2) depends on the phase error  $\theta$ , the SNR (the metric taken in the manuscript) becomes independent of phase error. Thus, there is no effect of phase on the SNR with single-element RIS as the effective channel is product of channel coefficients in each hop.

### III. STATISTICAL RESULTS FOR CASCADED CHANNELS

In this section, we develop statistical results of the multihop channels for both FSO and RF to facilitate average-value performance analysis of different metrics such as average BER. First, we require PDF and CDF of the cascaded FSO channels  $h = \prod_{i=1}^{K_1} h_i^{(tp)} = \prod_{i=1}^{K_1} h_i^{(t)} h_i^{(p)}$  and cascaded RF channels  $g = \prod_{i=1}^{K_2} g_i^{(f)}$ .

In the following two propositions, we express the PDF of dGG  $g_i^{(f)}$  and product of the dGG with pointing errors  $h_i^{(tp)}$  in terms of Fox's-H function without the limitation of integer-valued fading parameter due to the Meijer-G representation, as presented earlier [21], [22].

**Proposition 1.** The PDF of dGG distributed channel  $h_i^{(t)} = \chi_{i,1} \chi_{i,2}$ , where  $\chi_{i,1} \sim \mathcal{GG}(\alpha_{i,1}, \beta_{i,1}, \Omega_{i,1})$  and  $\chi_{i,2} \sim \mathcal{GG}(\alpha_{i,2}, \beta_{i,2}, \Omega_{i,2})$  can be expressed as

$$f_{h_i^{(t)}}(x) = \frac{x^{\alpha_{i,2} \beta_{i,2} - 1}}{\left(\frac{\Omega_{i,1}}{\beta_{i,1}}\right)^{\alpha_{i,1}} \left(\frac{\Omega_{i,2}}{\beta_{i,2}}\right)^{\beta_{i,2}} \Gamma(\beta_{i,1}) \Gamma(\beta_{i,2})} H_{0,2}^{2,0} \left[ \zeta_i x \mid \left(0, \frac{1}{\alpha_{i,2}}\right), \left(\frac{\alpha_{i,1} \beta_{i,1} - \alpha_{i,2} \beta_{i,2}}{\alpha_{i,1}}, \frac{1}{\alpha_{i,1}}\right) \right] \quad (7)$$

where  $\zeta_i = \left(\frac{\beta_{i,2}}{\Omega_{i,2}}\right)^{\frac{1}{\alpha_{i,2}}} \left(\frac{\beta_{i,1}}{\Omega_{i,1}}\right)^{\frac{1}{\alpha_{i,1}}}$ .

*Proof:* We use the Mellin's convolution to get the PDF of the product of two random variables as  $f_{h_i^{(t)}}(x) = \int_0^\infty \frac{1}{u} f_{\chi_{i,1}}\left(\frac{x}{u}\right) f_{\chi_{i,2}}(u) du$ , where the limits of the integral are selected using the inequalities  $0 \leq \frac{x}{u} \leq \infty$  and  $0 \leq u \leq \infty$  since  $\chi_1 \in [0, \infty)$  and  $\chi_2 \in [0, \infty)$ :

$$f_{h_i^{(t)}}(x) = \frac{\alpha_{i,1} \alpha_{i,2} x^{\alpha_{i,1} \beta_{i,1} - 1}}{\left(\frac{\Omega_{i,1}}{\beta_{i,1}}\right)^{\beta_{i,1}} \left(\frac{\Omega_{i,2}}{\beta_{i,2}}\right)^{\beta_{i,2}} \Gamma(\beta_{i,1}) \Gamma(\beta_{i,2})} \int_0^\infty u^{\alpha_{i,2} \beta_{i,2} - 1} u^{-\alpha_{i,1} \beta_{i,1}} \exp\left(-\frac{\beta_{i,1} x^{\alpha_{i,1}}}{u^{\alpha_{i,1}} \Omega_{i,1}}\right) \exp\left(-\frac{\beta_{i,2} u^{\alpha_{i,2}}}{\Omega_{i,2}}\right) du \quad (8)$$

Using  $u^{-\alpha_{i,1}} = t$  and the Meijer-G equivalent of the exponential function, we get

$$f_{h_i^{(t)}}(x) = \frac{\alpha_{i,2} x^{\alpha_{i,1} \beta_{i,1} - 1}}{\left(\frac{\Omega_{i,1}}{\beta_{i,1}}\right)^{\beta_{i,1}} \left(\frac{\Omega_{i,2}}{\beta_{i,2}}\right)^{\beta_{i,2}} \Gamma(\beta_{i,1}) \Gamma(\beta_{i,2})} \int_0^\infty t^{-\frac{\alpha_{i,2} \beta_{i,2}}{\alpha_{i,1}}} t^{\beta_{i,1} - 1} G_{0,1}^{1,0} \left[ \frac{\beta_{i,1} x^{\alpha_{i,1}}}{\Omega_{i,1}} t \mid - \right] G_{1,0}^{0,1} \left[ \frac{\Omega_{i,2}}{\beta_{i,2}} t^{\frac{\alpha_{i,2}}{\alpha_{i,1}}} \mid 1 \right] dt \quad (9)$$

We apply the identity [36, 07.34.21.0012.01] in (9) to get (7). The PDF of dGG distributed RF channel  $g_i^{(f)} = \chi_{i,3} \chi_{i,4}$ , where  $\chi_{i,3} \sim \mathcal{GG}(\alpha_{i,3}, \beta_{i,3}, \Omega_{i,3})$  and  $\chi_{i,4} \sim \mathcal{GG}(\alpha_{i,4}, \beta_{i,4}, \Omega_{i,4})$  has also of the form given by (7). ■

Unlike the Meijer's-G representation in the original work in [21], the derived PDF in (7) does not have integer-valued constraint on fading parameters of the dGG. The use of Fox's-H function for exact and asymptotic expressions for generalized fading models for wireless links is a popular choice among researchers. Recently, the computational software MATHEMATICA introduced the function  $FoxH$  for the computation of Fox's-H function.

As such, dGG model becomes Rayleigh fading with  $\alpha_{i,1} = \alpha_{i,2} = 1$  and  $\beta_{i,1} = \beta_{i,2} = 2$  and represents Nakagami-m fading for  $\alpha_{i,1} = \alpha_{i,2} = 1$  and  $\beta_{i,1} = \beta_{i,2} = 2m$ .

Next, we derive the PDF of the FSO link with the combined effect of dGG atmospheric turbulence and pointing errors:

**Proposition 2.** If the pointing error parameter  $h_i^{(p)}$  is distributed according to (4), then the PDF of the single FSO link

$h_i^{(tp)} = h_i^{(t)} h_i^{(p)}$  with atmospheric turbulence distributed as dGG and pointing errors is represented as

$$f_{h_i^{(tp)}}(x) = \frac{\rho_i^2 x^{\alpha_{i,2}\beta_{i,2}-1}}{A_{0,i}^{\alpha_{i,1}\beta_{i,2}} \left(\frac{\Omega_{i,1}}{\beta_{i,1}}\right)^{\frac{\alpha_{i,2}\beta_{i,2}}{\alpha_{i,1}}} \left(\frac{\Omega_{i,2}}{\beta_{i,2}}\right)^{\beta_{i,2}} \Gamma(\beta_{i,1}) \Gamma(\beta_{i,2})} H_{1,3}^{3,0} \left[ \frac{\zeta_i x}{A_{0,i}} \mid \begin{matrix} (\rho_i^2 - \alpha_{i,2}\beta_{i,2} + 1, 1) \\ V_1 \end{matrix} \right] \quad (10)$$

where  $\zeta_i = \left(\frac{\beta_{i,2}}{\Omega_{i,2}}\right)^{\frac{1}{\alpha_{i,2}}} \left(\frac{\beta_{i,1}}{\Omega_{i,1}}\right)^{\frac{1}{\alpha_{i,1}}}$  and  $V_1 = (0, \frac{1}{\alpha_{i,2}}), (\beta_{i,1} - \frac{\alpha_{i,2}\beta_{i,2}}{\alpha_{i,1}}, \frac{1}{\alpha_{i,1}}), (\rho_i^2 - \alpha_{i,2}\beta_{i,2}, 1)$ .

*Proof:* The combined PDF of dGG and pointing error can be expressed using the standard result on the product of two random variables

$$f_{h_i^{(tp)}}(x) = \int_0^{A_{0,i}} \frac{1}{u} f_{h_i^{(t)}}\left(\frac{x}{u}\right) f_{h_i^{(p)}}(u) du \quad (11)$$

where the integral limits are based on the inequalities  $0 \leq \frac{x}{u} \leq \infty$  and  $0 \leq u \leq A_0$  since  $h_i^{(t)} \in [0, \infty)$  and  $h_i^{(p)} \in [0, A_0]$ . Substituting (7) and (4) in (11) along with the definition of Fox-H function and applying the Fubini's theorem to interchange the integrals resulting into

$$f_{h_i^{(tp)}}(x) = \frac{\alpha_{i,2} x^{\alpha_{i,2}\beta_{i,2}-1}}{\left(\frac{\Omega_{i,1}}{\beta_{i,1}}\right)^{\frac{\alpha_{i,2}\beta_{i,2}}{\alpha_{i,1}}} \left(\frac{\Omega_{i,2}}{\beta_{i,2}}\right)^{\beta_{i,2}} \Gamma(\beta_{i,1}) \Gamma(\beta_{i,2})} \frac{\rho_i^2}{A_{0,i}^{\rho_i^2}} \frac{1}{2\pi j} \int_{\mathcal{L}} \left(\frac{\beta_{i,2}}{\Omega_{i,2}} \left(\frac{\beta_{i,1}}{\Omega_{i,1}}\right)^{\frac{\alpha_{i,2}}{\alpha_{i,1}}} (x)^{\alpha_{i,2}}\right)^s \Gamma(\beta_{i,1} - \frac{\alpha_{i,2}\beta_{i,2}}{\alpha_{i,1}} - \frac{\alpha_{i,2}}{\alpha_{i,1}} s) \Gamma(-s) \left(\int_0^{A_{0,i}} u^{\rho_i^2 - \alpha_{i,2}\beta_{i,2} - \alpha_{i,2}s - 1} du\right) ds \quad (12)$$

The inner integral of (12) is solved as  $\int_0^{A_{0,i}} u^{\rho_i^2 - \alpha_{i,2}\beta_{i,2} - \alpha_{i,2}s - 1} du = \frac{A_{0,i}^{\rho_i^2 - \alpha_{i,2}\beta_{i,2} - \alpha_{i,2}s}}{\rho_i^2 - \alpha_{i,2}\beta_{i,2} - \alpha_{i,2}s} = \frac{A_{0,i}^{\rho_i^2 - \alpha_{i,2}\beta_{i,2} - \alpha_{i,2}s}}{\rho_i^2 - \alpha_{i,2}\beta_{i,2} - \alpha_{i,2}s} \frac{\Gamma(\rho_i^2 - \alpha_{i,2}\beta_{i,2} - \alpha_{i,2}s)}{\Gamma(\rho_i^2 - \alpha_{i,2}\beta_{i,2} - \alpha_{i,2}s + 1)}$ . Further, we substitute the inner integral in (12), and use the integral representation of the Fox's H function and the identity [37, eq. 1.59] to get (10).

As a sanity check, we can integrate  $\int_0^\infty f_{h_i^{(tp)}}(x) dx$  to validate the derived PDF in (10) as

$$= \frac{\rho_i^2 \Gamma(\beta_{i,2}) \Gamma(\beta_{i,1}) \left(\frac{\beta_{i,2}}{\Omega_{i,2}}\right)^{-\beta_{i,2}} \left(\frac{\beta_{i,1}}{\Omega_{i,1}}\right)^{\frac{-\alpha_{i,2}\beta_{i,2}}{\alpha_{i,1}}}}{\left(\frac{\Omega_{i,1}}{\beta_{i,1}}\right)^{\frac{\alpha_{i,2}\beta_{i,2}}{\alpha_{i,1}}} \left(\frac{\Omega_{i,2}}{\beta_{i,2}}\right)^{\beta_{i,2}} \Gamma(\beta_{i,1}) \Gamma(\beta_{i,2}) \rho_i^2} = 1 \quad (13)$$

Note that PDF of [22] is a particular case of the Fox-H representation of the derived PDF in (10).

We then derive the PDF of the combined effect of IG shadowing and dGG fading for the RF link:

**Proposition 3.** The PDF of the single RF link  $g_i^{(sf)} = g_i^{(s)} g_i^{(f)}$  with the combined effect of shadowing and dGG is given by

$$f_{g_i^{(sf)}}(x) = \frac{x^{-1} (m_i - 1)^{m_i}}{\Gamma(\beta_{i,3}) \Gamma(\beta_{i,4})} H_{1,2}^{2,1} \left[ \frac{\zeta_i}{\sqrt{(m_i - 1)}} x \mid \left(\beta_{i,4}, \frac{1}{\alpha_{i,4}}\right), \left(\beta_{i,3}, \frac{1}{\alpha_{i,3}}\right) \right] \quad (14)$$

where  $\zeta_i = \left(\frac{\beta_{i,3}}{\Omega_{i,3}}\right)^{\frac{1}{\alpha_{i,3}}} \left(\frac{\beta_{i,4}}{\Omega_{i,4}}\right)^{\frac{1}{\alpha_{i,4}}}$ .

*Proof:* The combined PDF of dGG and shadowing can be expressed as

$$f_{g_i^{(sf)}}(x) = \int_0^\infty \frac{1}{u} f_{g_i^{(f)}}\left(\frac{x}{u}\right) f_{g_i^{(s)}}(u) du \quad (15)$$

Substituting (7) and (5) in (15) with the definition of Fox-H function and interchanging the integrals as per Fubini's theorem to get

$$f_{g_i^{(sf)}}(x) = \frac{x^{\alpha_{i,4}\beta_{i,4}-1}}{\left(\frac{\Omega_{i,3}}{\beta_{i,3}}\right)^{\frac{\alpha_{i,4}\beta_{i,4}}{\alpha_{i,3}}} \left(\frac{\Omega_{i,4}}{\beta_{i,4}}\right)^{\beta_{i,4}} \Gamma(\beta_{i,3}) \Gamma(\beta_{i,4})} \frac{1}{2\pi j} \int_{\mathcal{L}} \Gamma\left(-\frac{s}{\alpha_{i,4}}\right) \Gamma\left(\frac{\alpha_{i,3}\beta_{i,3} - \alpha_{i,4}\beta_{i,4}}{\alpha_{i,3}} - \frac{s}{\alpha_{i,3}}\right) (\zeta_i x)^s \left(\int_0^\infty u^{2m_i - \alpha_{i,4}\beta_{i,4} - s - 1} e^{-(m_i - 1)u^{-2}} du\right) ds \quad (16)$$

The inner integral of (16) is solved using the substitution  $t = (m_i - 1)u^{-2}$  as  $(m_i - 1) \frac{2m_i - \alpha_{i,4}\beta_{i,4} - s}{2} \int_0^\infty t^{\frac{s + \alpha_{i,4}\beta_{i,4} - 2m_i - 1}{2}} e^{-t} dt = (m_i - 1) \frac{2m_i - \alpha_{i,4}\beta_{i,4} - s}{2} \Gamma\left(\frac{s + \alpha_{i,4}\beta_{i,4} - 2m_i}{2}\right)$ . We substitute the inner integral in (16), and apply the definition of Fox-H with the identity [37, eq. 1.59] to get (14). ■

Finally we consider the effect of mobility in the last hop of RF-RIS i.e., from  $(K_2 - 1)$  RIS to destination.

**Proposition 4.** The resultant PDF of IG, dGG fading combined with mobility model for the last hop  $g_{K_2} = g_{K_2}^{(l)} g_{K_2}^{(s)} g_{K_2}^{(f)}$  is given as

$$f_{g_{K_2}}(x) = \frac{6x^{-1} (m_{K_2} - 1)^{m_{K_2}}}{\Gamma(\beta_{K_2,3}) \Gamma(\beta_{K_2,4})} H_{2,3}^{2,2} \left[ \frac{\zeta_{K_2}}{\sqrt{(m_{K_2} - 1)}} d_{K_2}^{\frac{\alpha}{2}} x \mid \left(1 + m_{K_2}, \frac{1}{2}\right), \left(-1, \frac{\alpha}{2}\right) \right] \quad (17)$$

where  $\zeta_{K_2} = \left(\frac{\beta_{K_2,4}}{\Omega_{K_2,4}}\right)^{\frac{1}{\alpha_{K_2,4}}} \left(\frac{\beta_{K_2,3}}{\Omega_{K_2,3}}\right)^{\frac{1}{\alpha_{K_2,3}}}$  and  $V_1 = (\beta_{K_2,4}, \frac{1}{\alpha_{K_2,4}}), (\beta_{K_2,3}, \frac{1}{\alpha_{K_2,3}}), (-3, \frac{\alpha}{2})$ .

*Proof:* The path loss component of last RF hop is  $g_{K_2}^{(l)} = r^{-\frac{\alpha}{2}}$ , where the PDF of  $r$  is given by (6). Now, the PDF of short-term fading combined with mobility model,  $g_{K_2} = g_{K_2}^{(l)} g_{K_2}^{(s)} g_{K_2}^{(f)}$  can be computed as

$$f_{g_{K_2}}(x) = \int_0^{d_{K_2}} f_{g_{K_2}}(x/r) f_r(r) dr \quad (18)$$

And the PDF of  $f_{g_{K_2}}(x/r)$  for a given  $r$  can be expressed as  $f_{g_{K_2}}(x/r) = r^{\frac{\alpha}{2}} f_{g_{K_2}^{(sf)}}(xr^{\frac{\alpha}{2}})$ , we substitute it in (18) and apply the integral representation of Fox's H-function and interchange the order of integration to get

$$f_{g_{K_2}}(x) = \frac{x^{-1} (m_{K_2} - 1)^{m_{K_2}}}{\Gamma(\beta_{K_2,3}) \Gamma(\beta_{K_2,4})} \frac{1}{2\pi j} \int_{\mathcal{L}_{K_2}} \left(\frac{\zeta_{K_2}}{\sqrt{m_{K_2} - 1}}\right)^{n_{K_2}} \Gamma(\beta_{K_2,4} - \frac{n_{K_2}}{\alpha_{K_2,4}}) \Gamma(\beta_{K_2,3} - \frac{n_{K_2}}{\alpha_{K_2,3}}) \Gamma(-m_{K_2} + \frac{n_{K_2}}{2}) x^{n_{K_2}} \left(\int_0^{d_{K_2}} 6r^{\frac{an_{K_2}}{2}} \left[\frac{r}{d_{K_2}^2} - \frac{r^2}{d_{K_2}^2}\right] dr\right) dn_{K_2} \quad (19)$$

Now, solving the inner integral as  $I = \frac{\Gamma(\frac{an_{K_2}}{2} + 2)}{\Gamma(\frac{an_{K_2}}{2} + 4)} d_{K_2}^{\frac{an_{K_2}}{2}}$ . We substitute it back and use the integral definition of Fox's H-function to get (17). ■

Next, we develop a framework to derive the PDF and CDF of cascaded channels  $h$  and  $g$ , as presented in Theorem 1:

**Theorem 1.** *If  $X_i$ ,  $i = 1 \dots K$  denote  $K$  i.n.i.d random variables with a PDF in the form of*

$$f_{X_i}(x) = \psi_i x^{\phi_i - 1} H_{p,q}^{m,n} \left[ \zeta_i x \mid \left\{ \begin{array}{l} (a_{i,j}, A_{i,j}) \\ (b_{i,j}, B_{i,j}) \end{array} \right\}_{j=1}^p \right] \quad (20)$$

then the PDF and CDF of the product of random variables  $X = \prod_{i=1}^K X_i$  are given by

$$f_X(x) = \frac{1}{x} \prod_{i=1}^K \psi_i \zeta_i^{-\phi_i} H_{Kp, Kq}^{K_m, K_n} \left[ \prod_{i=1}^K \zeta_i x \mid \left\{ \begin{array}{l} (a_{i,j} + A_{i,j} \phi_i, A_{i,j}) \\ (b_{i,j} + B_{i,j} \phi_i, B_{i,j}) \end{array} \right\}_{j=1}^p \right] \quad (21)$$

$$F_X(x) = \prod_{i=1}^K \psi_i \zeta_i^{-\phi_i} H_{Kp+1, Kq+1}^{K_m, K_n+1} \left[ \prod_{i=1}^K \zeta_i x \mid \left\{ \begin{array}{l} (1, 1), \{(a_{i,j} + A_{i,j} \phi_i, A_{i,j})\}_{j=1}^p \\ (b_{i,j} + B_{i,j} \phi_i, B_{i,j})\}_{j=1}^q \end{array} \right\}_{i=1}^K, (0, 1) \right] \quad (22)$$

*Proof:* The proof is presented in Appendix A. ■

Next, we use Theorem 1 to present the PDF and CDF of the cascaded FSO and RF channels realized through multiple RIS modules:

**Corollary 1.** *If  $h_i^{(tp)}$  is distributed according to (10), the PDF and CDF of cascaded FSO channel  $h = \prod_{i=1}^{K_1} h_i^{(tp)}$  are*

$$f_h(x) = \frac{1}{x} \psi_1 H_{K_1+1, 3K_1}^{3K_1, 0} \left[ U_1 x \mid \left\{ (\rho_i^2 + 1, 1) \right\}_1^{K_1} \right] \quad (23)$$

$$F_h(x) = \psi_1 H_{K_1+1, 3K_1+1}^{3K_1, 1} \left[ U_1 x \mid (1, 1), \left\{ (\rho_i^2 + 1, 1) \right\}_1^{K_1} \right] \quad (24)$$

where  $\psi_1 = \prod_{i=1}^{K_1} \frac{\rho_i^2}{\Gamma(\beta_{i,1})\Gamma(\beta_{i,2})}$ ,  $U_1 = \prod_{i=1}^{K_1} \frac{1}{A_{0,i}(\frac{\beta_{i,2}}{\Omega_{i,2}})^{\frac{1}{\alpha_{i,2}}} (\frac{\beta_{i,1}}{\Omega_{i,1}})^{\frac{1}{\alpha_{i,1}}}}$  and  $V_1 = \{(\beta_{i,1}, \frac{1}{\alpha_{i,1}}), (\beta_{i,2}, \frac{1}{\alpha_{i,2}}), (\rho_i^2, 1)\}_1^{K_1}$ .

*Proof:* A direct application of Theorem 1 proves the Corollary 1. ■

As a sanity check, to prove  $\int_0^\infty f_h(x) dx = 1$ , we use the identity [37, eq. 2.8]

$$\int_0^\infty f_h(x) dx = \psi_1 \prod_{i=1}^{K_1} \frac{\Gamma(\beta_{i,1})\Gamma(\beta_{i,1})\Gamma(\rho_i^2)}{\Gamma(\rho_i^2 + 1)} = 1 \quad (25)$$

**Corollary 2.** *The PDF and CDF of multi-hop RIS RF System which is the product of dGG combined with shadowing are given as*

$$f_g(x) = \frac{1}{x} \psi_2 H_{K_2+1, 2K_2+1}^{2K_2, K_2+1} \left[ U_2 x \mid \begin{array}{l} W_2 \\ V_2 \end{array} \right] \quad (26)$$

$$F_g(x) = \psi_2 H_{K_2+2, 2K_2+2}^{2K_2, K_2+2} \left[ U_2 x \mid \begin{array}{l} W_2, (1, 1) \\ V_2, (0, 1) \end{array} \right] \quad (27)$$

where  $\psi_2 = \prod_{i=1}^{K_2} \frac{(m_i-1)^{m_i}}{\Gamma(\beta_{i,3})\Gamma(\beta_{i,4})}$ ,  $U_2 = \prod_{i=1}^{K_2} \frac{(\frac{\beta_{i,4}}{\Omega_{i,4}})^{\frac{1}{\alpha_{i,4}}}}{(\frac{\beta_{i,3}}{\Omega_{i,3}})^{\frac{1}{\alpha_{i,3}}}} d_{K_2}^{\frac{\alpha}{2}} (\frac{\beta_{i,3}}{\Omega_{i,3}})^{\frac{1}{\alpha_{i,3}}}$ ,  $V_2 = \{(\beta_{i,3}, \frac{1}{\alpha_{i,3}}), (\beta_{i,4}, \frac{1}{\alpha_{i,4}})\}_1^{K_2}, (-3, \frac{\alpha}{2})$  and  $W_2 = \{(1 + m_i, \frac{1}{2})\}_1^{K_2}, (-1, \frac{\alpha}{2})$ .

*Proof:* A direct application of Theorem 1 completes the proof. ■

Using the IM/DD detector, the SNR of the cascaded FSO link is denoted by  $\gamma^{FSO} = \bar{\gamma}^{FSO} |h|^2$ , and the cascaded RF or R2V link as  $\gamma^{R2V} = \gamma^{RF} + \gamma^{LOS} = \bar{\gamma}^{RF} |g|^2 + \bar{\gamma}^{LOS} |g_{LOS}|^2$ , where  $\bar{\gamma}^{FSO} = \frac{P_1 |h_l|^2}{\sigma_R^2}$ ,  $\bar{\gamma}^{RF} = \frac{P_2 |g_l|^2}{\sigma_V^2}$  and  $\bar{\gamma}^{LOS} = \frac{P_2 |g_{LOS}^{(l)}|^2}{\sigma_V^2}$  are the SNR terms without fading for the FSO, RF and RF LOS links, respectively. Here,  $h_l = \prod_{i=1}^{K_1} h_i^{(l)}$  and  $g_l = \prod_{i=1}^{K_2} g_i^{(l)}$  are the overall path gain of the cascaded FSO links and RF links.

The PDF of SNR of cascaded RF links and LOS link can be expressed using mathematical transformation as  $f_{\gamma^{RF}}(\gamma) = \frac{1}{2\sqrt{\bar{\gamma}^{RF}} \gamma} f_g(\sqrt{\frac{\gamma}{\bar{\gamma}^{RF}}})$  and  $f_{\gamma^{LOS}}(\gamma) = \frac{1}{2\sqrt{\bar{\gamma}^{LOS}} \gamma} f_{g_{LOS}^{(sf)}}(\sqrt{\frac{\gamma}{\bar{\gamma}^{LOS}}})$  respectively.

We then compute the resultant PDF of RF SNR using inverse Laplace transform of moment generating function (MGF) of individual SNRs i.e.,  $f_{\gamma^{R2V}}(\gamma) = \frac{1}{2\pi j} \int_L M_{\gamma^{RF}}(s) M_{\gamma^{LOS}}(s) e^{s\gamma} ds$ . Now, MGF of individual SNRs are computed as

$$\begin{aligned} M_{\gamma^{RF}}(s) &= \int_0^\infty f_{\gamma^{RF}}(\gamma) e^{-s\gamma} d\gamma \\ &= \frac{\psi_2}{2} \int_0^\infty \gamma^{-1} H_{K_2+1, 2K_2+1}^{2K_2, K_2+1} \left[ U_2 \sqrt{\frac{\gamma}{\bar{\gamma}^{RF}}} \mid \left\{ (1 + m_i, \frac{1}{2}) \right\}_1^{K_2}, (-1, \frac{\alpha}{2}) \right] e^{-s\gamma} d\gamma \quad (28) \end{aligned}$$

Expanding the definition of Fox's H-function and solving the inner integral as  $\int_0^\infty \gamma^{\frac{n_1}{2}-1} e^{-s\gamma} d\gamma = n^{-\frac{n_1}{2}} \Gamma(\frac{n_1}{2})$ . Substituting it back, we get

$$\begin{aligned} M_{\gamma^{RF}}(s) &= \frac{\psi_2}{2} \frac{1}{2\pi j} \int_{\mathcal{L}_1} (U_2 \sqrt{\frac{1}{s\bar{\gamma}^{RF}}})^{n_1} \Gamma(\frac{n_1}{2}) \prod_{i=1}^{K_2} \Gamma(\beta_{i,4} - \frac{n_1}{\alpha_{i,4}}) \Gamma(\beta_{i,3} - \frac{n_1}{\alpha_{i,3}}) \Gamma(-m_i + \frac{n_1}{2}) \frac{\Gamma(\frac{\alpha n_1 + 2}{2})}{\Gamma(\frac{\alpha n_1 + 4}{2})} dn_1 \quad (29) \end{aligned}$$

Similarly, MGF of SNR of RF LOS link is given as

$$\begin{aligned} M_{\gamma^{LOS}}(s) &= \frac{\psi_{LOS}}{2} \frac{1}{2\pi j} \int_{\mathcal{L}_2} (U_{LOS} \sqrt{\frac{1}{s\bar{\gamma}^{LOS}}})^{n_2} \Gamma(-m_{LOS} + \frac{n_2}{2}) \\ &\Gamma(\frac{n_2}{2}) \Gamma(\beta_{LOS,4} - \frac{n_2}{\alpha_{LOS,4}}) \Gamma(\beta_{LOS,3} - \frac{n_2}{\alpha_{LOS,3}}) dn_2 \quad (30) \end{aligned}$$

where  $\psi_{LOS} = \frac{1}{\Gamma(\beta_{LOS,3})\Gamma(\beta_{LOS,4})}$  and  $U_{LOS} = \frac{(\frac{\beta_{LOS,4}}{\Omega_{LOS,4}})^{\frac{1}{\alpha_{LOS,4}}}}{\sqrt{(m_{LOS}-1)}} \frac{1}{\Gamma(\beta_{LOS,3})} (\frac{\beta_{LOS,3}}{\Omega_{LOS,3}})^{\frac{1}{\alpha_{LOS,3}}}$ .

Now, the inner integral of PDF of resultant SNR becomes  $\frac{1}{2\pi j} \int_L s^{-\frac{n_1}{2} - \frac{n_2}{2}} e^{s\gamma} ds = \frac{\gamma^{\frac{n_1}{2} + \frac{n_2}{2} - 1}}{\Gamma(\frac{n_1}{2} + \frac{n_2}{2})}$ . We substitute it back and apply the definition of bi-variate Fox's H-function, we get

$$\begin{aligned} f_{\gamma^{R2V}}(\gamma) &= \frac{\psi_2 \psi_{LOS}}{4} \gamma^{-1} H_{0,1:K_2+2, 2K_2+1; 2, 2}^{0, 0: 2K_2, K_2+2; 2, 2} \\ &\left[ U_2 \sqrt{\frac{\gamma}{\bar{\gamma}^{RF}}} \mid \begin{array}{l} - : W_2; W_{LOS} \\ U_{LOS} \sqrt{\frac{\gamma}{\bar{\gamma}^{LOS}}} \mid (1 : \frac{1}{2}, \frac{1}{2}) : V_2 : V_{LOS} \end{array} \right] \quad (31) \end{aligned}$$

where  $W_2 = \{(1 + m_i, \frac{1}{2})\}_1^{K_2}, (-1, \frac{\alpha}{2}), (1, \frac{1}{2}), V_2 = \{(\beta_{i,3}, \frac{1}{\alpha_{i,3}}), (\beta_{i,4}, \frac{1}{\alpha_{i,4}})\}_1^{K_2}, (-3, \frac{\alpha}{2}), W_{LOS} = (1 + m_{LOS}, \frac{1}{2}), (1, \frac{1}{2})$  and  $V_{LOS} = (\beta_{LOS,3}, \frac{1}{\alpha_{LOS,3}}), (\beta_{LOS,4}, \frac{1}{\alpha_{LOS,4}})$ .

Similarly, CDF of the resultant SNR can be obtained as  $F_{\gamma^{R2V}}(\gamma) = \frac{1}{2\pi j} \int_L M_{\gamma^{RF}}(s) M_{\gamma^{LOS}}(s) s^{-1} e^{s\gamma} ds$

$$\begin{aligned} F_{\gamma^{R2V}}(\gamma) &= \frac{\psi_2 \psi_{LOS}}{4} H_{0,1:K_2+2, 2K_2+1; 2, 2}^{0, 0: 2K_2, K_2+2; 2, 2} \\ &\left[ U_2 \sqrt{\frac{\gamma}{\bar{\gamma}^{RF}}} \mid \begin{array}{l} - : W_2; W_{LOS} \\ U_{LOS} \sqrt{\frac{\gamma}{\bar{\gamma}^{LOS}}} \mid (0 : \frac{1}{2}, \frac{1}{2}) : V_2 : V_{LOS} \end{array} \right] \quad (32) \end{aligned}$$

In the following section, we analyze the system performance employing fixed-gain AF relaying to integrate the FSO link with vehicular transmissions over RF.

#### IV. FIXED-GAIN AF RELAYING FOR MIXED SYSTEM

In this section, we analyze the mixed system by employing the fixed-gain AF relaying protocol to the received FSO signal forwarding the signal over RF to the desired vehicle. In contrast to the channel-assisted AF relaying, gain applied at the relay in the fixed-gain relaying protocol is computed using received signal from the source to the relay. The fixed-gain AF relaying is relatively simpler in terms of computational complexity due to the relaxation on the knowledge of the perfect channel state information. The resultant SNR of the mixed system comprising of FSO and RF links can be expressed as [30]:

$$\gamma^{AF} = \frac{\gamma^{FSO}\gamma^{R2V}}{\gamma^{R2V} + C} \quad (33)$$

where  $C = P_2/G^2\sigma_w^2$ . Applying the theory of random variables on (33), the PDF of  $\gamma^{AF}$  is:

$$f_{\gamma^{AF}}(\gamma) = \int_0^\infty f_{\gamma^{FSO}}\left(\frac{\gamma(x+C)}{x}\right) f_{\gamma^{R2V}}(x) \frac{x+C}{x} dx \quad (34)$$

where  $f_{\gamma^{FSO}}(\gamma)$  and  $f_{\gamma^{R2V}}(\gamma)$  are the PDF of SNR for FSO and RF links, respectively. We use (23) and (26) with a simple transformation of random variable to get the PDF of SNR for FSO  $f_{\gamma^{FSO}}(\gamma) = \frac{1}{2\sqrt{\gamma}\sqrt{\gamma^{FSO}}} f_h(\sqrt{\frac{\gamma}{\gamma^{FSO}}})$  and RF link  $f_{\gamma^{R2V}}(\gamma) = \frac{1}{2\sqrt{\gamma}\sqrt{\gamma^{R2V}}} f_g(\sqrt{\frac{\gamma}{\gamma^{R2V}}})$ .

**Lemma 1.** *The PDF and CDF of the fixed-gain AF relaying system in (34) is given as*

$$f_{\gamma^{AF}}(\gamma) = \frac{1}{8\gamma} \psi_1 \psi_2 \psi_{LOS} H_{1,0:3K_1, K_1+1; K_2+2, 2K_2+1; 2, 2}^{0,1; 0,3K_1, 2K_2, K_2+2; 2, 2} \left[ \begin{array}{c} U_1^{-1} \sqrt{\frac{\gamma^{FSO}}{\gamma}} \\ U_2 \sqrt{\frac{C}{\gamma^{RF}}} \\ U_{LOS} \sqrt{\frac{C}{\gamma^{LOS}}} \end{array} \middle| \begin{array}{c} (1 : \frac{1}{2}, \frac{1}{2}, \frac{1}{2}) : V_1; W_2; W_{LOS} \\ - : W_1, (1, \frac{1}{2}); V_2; V_{LOS} \end{array} \right] \quad (35)$$

$$F_{\gamma^{AF}}(\gamma) = \frac{1}{8} \psi_1 \psi_2 \psi_{LOS} H_{1,0:3K_1+1, K_1+2; K_2+2, 2K_2+1; 2, 2}^{0,1; 1,3K_1, 2K_2, K_2+2; 2, 2} \left[ \begin{array}{c} U_1^{-1} \sqrt{\frac{\gamma^{FSO}}{\gamma}} \\ U_2 \sqrt{\frac{C}{\gamma^{RF}}} \\ U_{LOS} \sqrt{\frac{C}{\gamma^{LOS}}} \end{array} \middle| \begin{array}{c} (1 : \frac{1}{2}, \frac{1}{2}, \frac{1}{2}) : V_1, (1, \frac{1}{2}); W_2; W_{LOS} \\ - : (0, \frac{1}{2}), W_1, (1, \frac{1}{2}); V_2; V_{LOS} \end{array} \right] \quad (36)$$

where  $V_1 = \{(1 - \beta_{i,1}, \frac{1}{\alpha_{i,1}}), (1 - \beta_{i,2}, \frac{1}{\alpha_{i,2}}), (1 - \rho_i^2, 1)\}_1^{K_1}$ ,  $W_1 = \{(-\rho_i^2, 1)\}_1^{K_1}$ ,  $V_2 = \{(\beta_{i,3}, \frac{1}{\alpha_{i,3}}), (\beta_{i,4}, \frac{1}{\alpha_{i,4}})\}_1^{K_2}$ ,  $W_2 = \{(1 + m_i, \frac{1}{2})\}_1^{K_2}$ ,  $(-1, \frac{a}{2}), (1, \frac{1}{2})$ ,  $W_{LOS} = (1 + m_{LOS}, \frac{1}{2}), (1, \frac{1}{2})$  and  $V_{LOS} = (\beta_{LOS,3}, \frac{1}{\alpha_{LOS,3}}), (\beta_{LOS,4}, \frac{1}{\alpha_{LOS,4}})$ .

*Proof:* We substitute PDF of FSO and RF links in (34), use the integral representation of the Fox's-H function and interchanging the order of integration to express

$$f_{\gamma^{AF}}(\gamma) = \frac{\psi_1 \psi_2 \psi_{LOS}}{8\gamma} \frac{1}{(2\pi j)^3} \int_{\mathcal{L}_1} \int_{\mathcal{L}_2} \int_{\mathcal{L}_3} (U_1 \sqrt{\frac{\gamma}{\gamma^{FSO}}})^{-n_1} \prod_{i=1}^{K_1} \Gamma(\beta_{i,2} + \frac{n_1}{\alpha_{i,2}}) \Gamma(\beta_{i,1} + \frac{n_1}{\alpha_{i,1}}) \frac{\Gamma(\rho_i^2 + n_1)}{\Gamma(\rho_i^2 + n_1 + 1)} \left( U_2 \sqrt{\frac{1}{\gamma^{RF}}} \right)^{-n_2} \prod_{i=1}^{K_2} \Gamma(\beta_{i,4} + \frac{n_2}{\alpha_{i,4}}) \Gamma(\beta_{i,3} + \frac{n_2}{\alpha_{i,3}}) \Gamma(-m_i - \frac{n_2}{2}) \Gamma(-\frac{n_2}{2}) \frac{\Gamma(-\frac{an_2}{2} + 2)}{\Gamma(-\frac{an_2}{2} + 4)} \left( U_{LOS} \sqrt{\frac{1}{\gamma^{LOS}}} \right)^{-n_3} \Gamma(\beta_{LOS,4} + \frac{n_3}{\alpha_{LOS,4}}) \Gamma(\beta_{LOS,3} + \frac{n_3}{\alpha_{LOS,3}}) \Gamma(-m_{LOS} - \frac{n_3}{2}) \frac{\Gamma(-\frac{n_3}{2})}{\Gamma(\frac{n_2}{2} + \frac{n_3}{2})} \left( \int_0^\infty x^{-1 - \frac{n_2}{2} - \frac{n_3}{2}} \left( \frac{x+C}{x} \right)^{-\frac{n_1}{2}} dx \right) dn_1 dn_2 dn_3 \quad (37)$$

We use the identities [38, (3.194/3)] and [38, (8.384/1)] to express inner integral in terms of Gamma function:

$$\int_0^\infty x^{-1 - \frac{n_2}{2} - \frac{n_3}{2}} \left( \frac{x+C}{x} \right)^{-\frac{n_1}{2}} dx = \frac{C^{-\frac{n_2}{2} - \frac{n_3}{2}} \Gamma(\frac{n_2}{2} + \frac{n_3}{2}) \Gamma(-\frac{n_2}{2} - \frac{n_3}{2} + \frac{n_1}{2})}{\Gamma(\frac{n_1}{2})} \quad (38)$$

Substituting (38) in (37) and applying the definition of trivariate Fox's-H function, we get (35).

To develop an analytical expression for the CDF, we use (35) in  $F_{\gamma^{AF}}(\gamma) = \int_0^\gamma f_{\gamma^{AF}}(t) dt$ , apply the definition of Fox's-H function to solve  $\int_0^\gamma t^{\frac{n_1}{2}-1} dt = \gamma^{\frac{n_1}{2}} \frac{2}{n_1} = \gamma^{\frac{n_1}{2}} \frac{\Gamma(\frac{n_1}{2})}{\Gamma(1 + \frac{n_1}{2})}$ , and then use the definition of trivariate Fox's-H function, to get (36), which completes the proof of Lemma. ■

Note that trivariate Fox's H-function has been extensively used for the representation of complicated fading distribution functions. Moreover, numerical computational codes are available in MATLAB for the computation of trivariate Fox's H-function.

Next, we use the results of Lemma 1 to present analytical expressions of outage probability, and average BER of the integrated FSO-RF system equipped with multiple RIS.

#### A. Outage Probability

The outage probability of a system is a probabilistic measure of the instantaneous SNR falling below certain threshold SNR  $\gamma_{th}$  i.e.,  $P_{out} = Pr(\gamma \leq \gamma_{th}) = F_\gamma(\gamma_{th})$ . Thus, an exact outage probability for the mixed FSO-RF system can be simply expressed using  $\gamma = \gamma_{th}$  in the CDF formulation  $F_{\gamma^{AF}}(\gamma)$  of (36).

We use [39] to compute the residue of the trivariate Fox's H-function at the dominant poles of (36) to develop the asymptotic expression in the high SNR regime, as given in (39). The first term of (39) corresponds to the residue at dominant pole of FSO coefficients represented by  $p_1 = \min\{\{\frac{\beta_{i,1}\alpha_{i,1}}{2}, \frac{\beta_{i,2}\alpha_{i,2}}{2}, \frac{\rho_i^2}{2}\}_1^{K_1}\}$  and later terms represent residues corresponding to RF coefficients at dominant poles  $p_2 = \min\{\{\frac{\beta_{i,3}\alpha_{i,3}}{2}, \frac{\beta_{i,4}\alpha_{i,4}}{2}\}_1^{K_2}\}$  and

$$\begin{aligned}
P_{\text{out}}^{AF,\infty} &\approx \frac{\psi_1\psi_2\psi_{LOS}}{8} \Gamma\left(\frac{p_2}{2} + \frac{p_3}{2} + \frac{p_1}{2}\right) \left[ \left( U_1^{-1} \sqrt{\frac{\gamma^{FSO}}{\gamma_{th}}} \right)^{-p_1} \prod_{i=1}^{K_1} \frac{2}{p_1} \Gamma\left(\beta_{i,2} - \frac{p_1}{\alpha_{i,2}}\right) \Gamma\left(\beta_{i,1} - \frac{p_1}{\alpha_{i,1}}\right) \frac{\Gamma(\rho_i^2 - p_1)}{\Gamma(\rho_i^2 - p_1 + 1)\Gamma(-\frac{p_1}{2})} \right] \\
&\left[ \left( U_2 \sqrt{\frac{C}{\gamma_{RF}}} \right)^{p_2} \prod_{i=1}^{K_2} \Gamma\left(\beta_{i,4} - \frac{p_2}{\alpha_{i,4}}\right) \Gamma\left(\beta_{i,3} - \frac{p_2}{\alpha_{i,3}}\right) \Gamma\left(\frac{p_2}{2}\right) \Gamma\left(-m_i + \frac{p_2}{2}\right) \frac{\Gamma\left(\frac{ap_2}{2} + 2\right)}{\Gamma\left(\frac{ap_2}{2} + 4\right)} \right] \\
&\left( U_{LOS} \sqrt{\frac{C}{\gamma_{LOS}}} \right)^{p_3} \Gamma\left(\frac{p_3}{2}\right) \Gamma\left(\beta_{LOS,4} - \frac{p_3}{\alpha_{LOS,4}}\right) \Gamma\left(\beta_{LOS,3} - \frac{p_3}{\alpha_{LOS,3}}\right) \Gamma\left(-m_{LOS} + \frac{p_3}{2}\right) \quad (39)
\end{aligned}$$

$p_3 = \min\left\{\frac{\beta_{LOS,3}\alpha_{LOS,3}}{2}, \frac{\beta_{LOS,4}\alpha_{LOS,4}}{2}\right\}$ . To get the diversity order  $G_{\text{out}}$  of the considered system, we express (39) as  $P_{\text{out}}^{AF,\infty} \propto \gamma_0^{-G_{\text{out}}}$ . Finally, selection of dominant poles in (39) gives rise to the outage diversity order of the systems as  $G_{\text{out}} = p_1 + p_2 + p_3$ . The derived diversity order depicts that the performance of the considered multi-hop transmission depends on the link with the minimum of channel parameters. Thus, a performance degradation due to the channel fading and pointing errors can be compensated with an increase in the number of RISs for a given distance in both links.

### B. Average BER

Using the CDF of the SNR, the average BER of a communication system is given by [40]:

$$\bar{P}_e = \frac{q^p}{2\Gamma(p)} \int_0^\infty \gamma^{p-1} e^{-q\gamma} F_\gamma(\gamma) d\gamma \quad (40)$$

where  $p$  and  $q$  parameterize different modulation schemes.

We substitute (36) in (40) and use the trivariate Fox's-H function [37] definition, express the inner integral as  $\int_0^\infty \gamma^{p-\frac{n_1}{2}-1} e^{-q\gamma} d\gamma = \frac{\Gamma(p-\frac{n_1}{2})}{q^{p-\frac{n_1}{2}}}$ , and again apply the definition of trivariate Fox's-H function to express the average BER of the integrated system as

$$\begin{aligned}
P_e^{\bar{AF}} &= \frac{1}{16\Gamma(p)} \psi_1\psi_2\psi_{LOS} H_{1,0:3K_1+1,K_1+3;K_2+2,2K_2+1;2,2}^{0,1;2,3K_1;2K_2,K_2+2;2,2} \\
&\left[ \begin{array}{c} U_1^{-1} \sqrt{q\gamma^{FSO}} \\ U_2 \sqrt{\frac{C}{\gamma_{RF}}} \\ U_{LOS} \sqrt{\frac{C}{\gamma_{LOS}}} \end{array} \middle| \begin{array}{c} (1 : \frac{1}{2}, \frac{1}{2}, \frac{1}{2}) : V_1; W_2; W_{LOS} \\ - : W_1; V_2; V_{LOS} \end{array} \right] \quad (41)
\end{aligned}$$

where  $V_1 = \{(1 - \beta_{i,1}, \frac{1}{\alpha_{i,1}}), (1 - \beta_{i,2}, \frac{1}{\alpha_{i,2}}), (1 - \rho_i^2, 1)\}_1^{K_1}, (1, \frac{1}{2}), W_1 = (p, \frac{1}{2}), (0, \frac{1}{2}), \{(-\rho_i^2, 1)\}_1^{K_1}, (1, \frac{1}{2}), V_2 = \{(\beta_{i,3}, \frac{1}{\alpha_{i,3}}), (\beta_{i,4}, \frac{1}{\alpha_{i,4}})\}_1^{K_2}, (-3, \frac{a}{2}), W_2 = \{(1 + m_i, \frac{1}{2})\}_1^{K_2}, (-1, \frac{a}{2}), (1, \frac{1}{2}), W_{LOS} = (1 + m_{LOS}, \frac{1}{2}), (1, \frac{1}{2})$  and  $V_{LOS} = (\beta_{LOS,3}, \frac{1}{\alpha_{LOS,3}}), (\beta_{LOS,4}, \frac{1}{\alpha_{LOS,4}})$ .

Note that an asymptotic expression for the average BER can be derived using the similar procedure applied for the outage probability (expressions are not listed due to the space constraint).

Similarly, ergodic capacity for the mixed system can be derived applying mathematical procedure as developed through average BER derivation (omitted here because of the page constraints).

## V. DF RELAYING FOR MIXED SYSTEM

Although the fixed-gain AF relaying is a simple technique to implement, it is desirable to analyze the performance of the near-optimal DF protocol as a benchmark for the system performance.

Since  $\gamma^{FSO}$  and  $\gamma^{R2V}$  are independent, the end-to-end SNR of DF relaying system is given as  $\gamma = \min\{\gamma^{FSO}, \gamma^{R2V}\}$ . Hence, the CDF of the SNR is

$$F_\gamma^{DF}(\gamma) = F_{\gamma^{FSO}}(\gamma) + F_{\gamma^{R2V}}(\gamma) - F_{\gamma^{FSO}}(\gamma)F_{\gamma^{R2V}}(\gamma) \quad (42)$$

### A. Outage Probability

Similar to the fixed-gain, an exact outage probability for the integrated FSO-RF system can be expressed using the CDF at a specific threshold value of SNR  $P_{\text{out}}^{DF} = F_\gamma^{DF}(\gamma_{th})$ . Further, we use the series expansion of Fox's H-function [39, Th. 1.11] to represent the outage probability in the high SNR regime, as given in (43).

### B. Average BER

For the DF based dual-hop FSO-RF system, the average BER can be expressed using the average BER of individual links [41]:

$$\bar{P}_e = \bar{P}_e^{(FSO)} + \bar{P}_e^{(R2V)} - 2\bar{P}_e^{(FSO)}\bar{P}_e^{(R2V)} \quad (44)$$

where  $\bar{P}_e^{(FSO)}$  and  $\bar{P}_e^{(R2V)}$  are average BER of the cascaded FSO and cascaded RF links, respectively.

To derive  $\bar{P}_e^{(FSO)}$ , we substitute  $F_{\gamma^{FSO}}(\gamma)$  in (40), expand the definition of Fox's-H function and interchange the order of integration to solve the inner integral  $\int_0^\infty \gamma^{p+\frac{n_1}{2}-1} e^{-q\gamma} d\gamma = \frac{\Gamma(p+\frac{n_1}{2})}{q^{p+\frac{n_1}{2}}}$ . We then apply the definition of Fox's-H function to get

$$\bar{P}_e^{(FSO)} = \frac{\psi_1}{2\Gamma(p)} H_{K_1+2,3K_1+1}^{3K_1,2} \left[ \frac{U_1}{\sqrt{q\gamma^{FSO}}} \middle| \begin{array}{c} (1, 1), V \\ V_1, (0, 1) \end{array} \right] \quad (45)$$

where  $\psi_1 = \prod_{i=1}^{K_1} \frac{\rho_i^2}{\Gamma(\beta_{i,1})\Gamma(\beta_{i,2})}$ ,  $U_1 = \prod_{i=1}^{K_1} \frac{1}{A_{0,i}} \left(\frac{\beta_{i,2}}{\Omega_{i,2}}\right)^{\frac{1}{\alpha_{i,2}}} \left(\frac{\beta_{i,1}}{\Omega_{i,1}}\right)^{\frac{1}{\alpha_{i,1}}}$ ,  $V = (1-p, \frac{1}{2}), \{(\rho_i^2+1, 1)\}_1^{K_1}$  and  $V_1 = \{(\beta_{i,1}, \frac{1}{\alpha_{i,1}}), (\beta_{i,2}, \frac{1}{\alpha_{i,2}}), (\rho_i^2, 1)\}_1^{K_1}$ .

Similarly, the average BER of the RF link is:

$$\begin{aligned}
\bar{P}_e^{(R2V)} &= \frac{1}{8\Gamma(p)} \psi_2\psi_{LOS} H_{1,1:K_2+2,2K_2+1;2,2}^{0,1;2K_2,K_2+2;2,2} \\
&\left[ \begin{array}{c} U_2 \sqrt{\frac{1}{q\gamma_{RF}}} \\ U_{LOS} \sqrt{\frac{1}{q\gamma_{LOS}}} \end{array} \middle| \begin{array}{c} (1-p, \frac{1}{2}, \frac{1}{2}) : W_2; W_{LOS} \\ (0 : \frac{1}{2}, \frac{1}{2}) : V_2 : V_{LOS} \end{array} \right] \quad (46)
\end{aligned}$$

$$\begin{aligned}
P_{\text{out}}^{\infty} \approx & \frac{\psi_1}{2} \left[ \left( U_1^{-1} \sqrt{\frac{\bar{\gamma}^{FSO}}{\gamma_{th}}} \right)^{-p_1} \prod_{i=1}^{K_1} \frac{2}{p_1} \Gamma(\beta_{i,2} - \frac{p_1}{\alpha_{i,2}}) \Gamma(\beta_{i,1} - \frac{p_1}{\alpha_{i,1}}) \frac{\Gamma(\rho_i^2 - p_1)}{\Gamma(\rho_i^2 - p_1 + 1) \Gamma(-\frac{p_1}{2})} \right] + \\
& \frac{\psi_2 \psi_{LOS}}{4} \Gamma(\frac{p_2}{2} + \frac{p_3}{2}) \left[ \left( U_2 \sqrt{\frac{C}{\bar{\gamma}^{RF}}} \right)^{p_2} \prod_{i=1}^{K_2} \Gamma(\beta_{i,4} - \frac{p_2}{\alpha_{i,4}}) \Gamma(\beta_{i,3} - \frac{p_2}{\alpha_{i,3}}) \Gamma(\frac{p_2}{2}) \Gamma(-m_i + \frac{p_2}{2}) \frac{\Gamma(\frac{\alpha p_2}{2} + 2)}{\Gamma(\frac{\alpha p_2}{2} + 4)} \right. \\
& \left. \left( U_{LOS} \sqrt{\frac{C}{\bar{\gamma}^{LOS}}} \right)^{p_3} \Gamma(\frac{p_3}{2}) \Gamma(\beta_{LOS,4} - \frac{p_3}{\alpha_{LOS,4}}) \Gamma(\beta_{LOS,3} - \frac{p_3}{\alpha_{LOS,3}}) \Gamma(-m_{LOS} + \frac{p_3}{2}) \right] \quad (43)
\end{aligned}$$

where  $W_2 = \{(1 + m_i, \frac{1}{2})\}_1^{K_2}, (-1, \frac{a}{2}), (1, \frac{1}{2}),$   
 $V_2 = \{(\beta_{i,3}, \frac{1}{\alpha_{i,3}}), (\beta_{i,4}, \frac{1}{\alpha_{i,4}})\}_1^{K_2}, (-3, \frac{a}{2}),$   
 $W_{LOS} = (1 + m_{LOS}, \frac{1}{2}), (1, \frac{1}{2})$  and  $V_{LOS} =$   
 $(\beta_{LOS,3}, \frac{1}{\alpha_{LOS,3}}), (\beta_{LOS,4}, \frac{1}{\alpha_{LOS,4}}).$

The asymptotic expressions for average BER can be derived applying the similar procedure as adopted for the outage probability.

## VI. NUMERICAL AND SIMULATION ANALYSIS

This section demonstrates the performance of multiple RIS empowered vehicular communications and validates the mathematical performance metrics using Monte-Carlo simulations. We use MATLAB and MATHEMATICA computational software for computer simulations. We also demonstrate the tightness of asymptotic expressions at a high SNR and verify the diversity order of the system by varying channel fading parameters. We assume that the backhaul FSO link length is  $d_1 = 1000$  m (a typical backhaul scenario for FSO in urban area) and  $K_1 - 1$  optical RISs are deployed at equal distances. We also show the effect of unequal deployment of RIS-FSO in Fig. 6. We model the FSO atmospheric turbulence using dGG parameters corresponding to strong turbulence (ST) ( $\alpha_1 = 1.8621, \alpha_2 = 1, \beta_1 = 0.5, \beta_2 = 1.8, \Omega_1 = 1.5074, \Omega_2 = 0.928$ ) and moderate turbulence (MT) ( $\alpha_1 = 2.169, \alpha_2 = 1, \beta_1 = 0.55, \beta_2 = 2.35, \Omega_1 = 1.5793, \Omega_2 = 0.9671$ ) [22]. We compute the effective path loss for FSO links for a visibility range of 3 Km [42] (a commonly used value in hazy conditions) at a wavelength 1550 nm. We take values of detector responsivity is 0.41 A/W and AWGN noise variance of  $10^{-14}$  A<sup>2</sup>/GHz. We consider pointing error parameter  $\rho = 2.5$  at  $K_1 = 2$  and low or negligible pointing error ( $\rho = 5$ ) at higher  $K_1$  due to perfect beam alignment.

To illustrate the vehicular communications, we use the link distance of  $d_2 = 100$ m with the orientation of RF-RIS, as shown in Fig. 1 by deploying  $K_2 - 1$  RISs at equal distances. The use of 100m RIS-assisted vehicular link is considered to accommodate a typical cluttered environment in high-traffic scenarios, for example, near the shopping mall and traffic light junctions. We use the equal distance placement of RF-RIS for the proposed scheme to have a higher resultant path loss [43, eq. 5] for better performance comparison. In Fig. 6, we also considered a higher vehicular link of 300 m and compared the performance between unequal and equal distance placement of RF-RIS modules. We use RF dGG parameters  $\alpha_3 = 1.5, \alpha_4 = 1, \beta_3 = 1.5, \beta_4 = 1.5, \Omega_3 = 1.5793, \Omega_4 = 0.9671$  to model the R2V link for vehicular transmissions [25]. We use shadowing parameter  $m = 1.2, 7.4, 15$  corresponding to  $K_2 = 2, 3, 5$  hops to model the the effect of shadowing in the presence of obstacles [34]. The lower the parameter  $m$ , the higher the effect of shadowing. In addition, we also vary the path loss

exponent  $a$  w.r.t  $K_2$  and in particular, we consider  $a = 4, 3, 2$  at  $K_2 = 2, 3, 5$  respectively. For the direct link, we use same fading parameters with shadowing  $m = 1.2$  and path loss exponent  $a = 4$ . To simulate the path gain of the R2V link, we use equal gain of transmit and receive antenna as  $G_t = G_r = 25$  dBi at a frequency of 800 MHz. These parameters are selected to ensure that the both FSO and R2V have similar average SNR to avoid imbalance of the two links. Indeed, the change in carrier frequency impacts the path loss, and a different carrier frequency will change the results without a significant change in the comparative study. The variance of AWGN is considered to be  $-104.4$  dBm with a channel bandwidth of 20 MHz. For RF-RIS, the wavelength at 800 MHz is 37.5 cm. Since the dimension of RIS element is proportional to wavelength, the RIS element has a dimension of  $37.5\text{cm} \times 37.5\text{cm}$ . The size of FSO RIS is equal to the diameter of the receiver aperture, usually taken as 20cm [12].

First, we demonstrate the effect of multiple RISs for both FSO (with moderate turbulence) and vehicular transmissions by plotting outage probability (in Fig. 2(a)), and average BER for differential binary phase shift keying ( $p = 1$  and  $q = 1$ ) (in Fig. 2(b)) considering the same turbulence, pointing errors, and fading scenarios in each hop. Figures show the performance of multi-RIS system versus number of RISs ( $K_1 = K_2 = K$ ,  $K - 1$  RISs constituting  $K$  hops) for FSO and R2V transmissions at a transmit power of  $P_t = 30$  dBm and  $P_t = 50$  dBm. We consider two pointing error (PE) scenarios: PE1, and PE2. In PE1, we assume that all the FSO links undergo the same pointing errors  $\rho = 2.5$ . In PE2, we use higher pointing error parameters ( $\rho = 1$  or  $\rho = 2.5$ ) from the source transmitter to the first optical RIS and last optical RIS to the relay and negligible pointing errors involving RIS to RIS due to a perfect beam alignment. The figure shows that an increase in the number of RIS modules between a source and destination decreases the performance, which can be regarded as a counter productive. However, without the use of multiple RIS, there exists no direct link which precludes any FSO transmissions and highly degraded R2V links. Thus, the use of multi-RIS should be limited enabling line-of-sight transmissions. Note that the reason for degradation in the performance with an increase in the number of RIS modules is the manifestation of cascading of channel coefficients comprising deterministic path gain ( $h_l < 1$ ). It should be mentioned that the use of multiple RIS is applied in the same channel conditions without harnessing the LOS, depicting a degradation in the performance with multiple RIS. For a fair comparison in the multihop scenario, an increase in the number of RIS may enjoy better channel conditions resulting in improved performance, as illustrated below.

Next, we consider a more practical setup with different fading scenarios in each hop to demonstrate the use of multiple

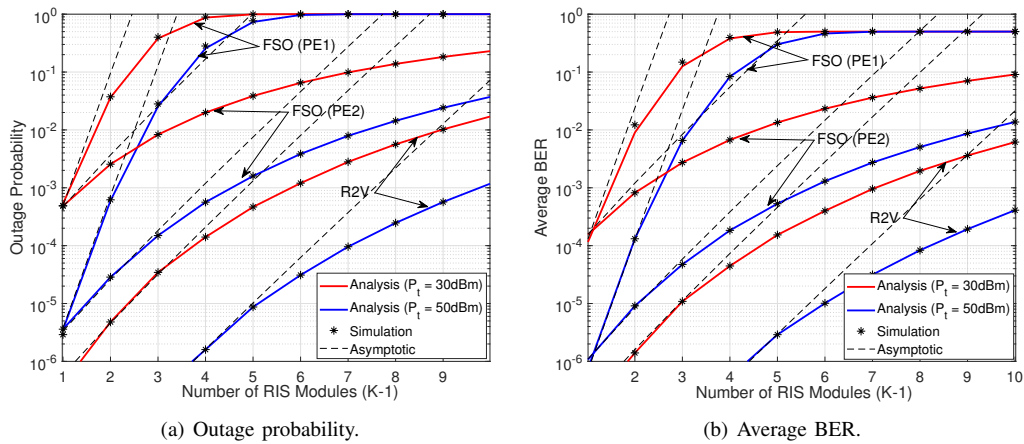


Fig. 2. Performance demonstration of multi-RIS transmissions for FSO and R2V links ( $K_1 = K_2 = K$ ) under similar channel conditions.

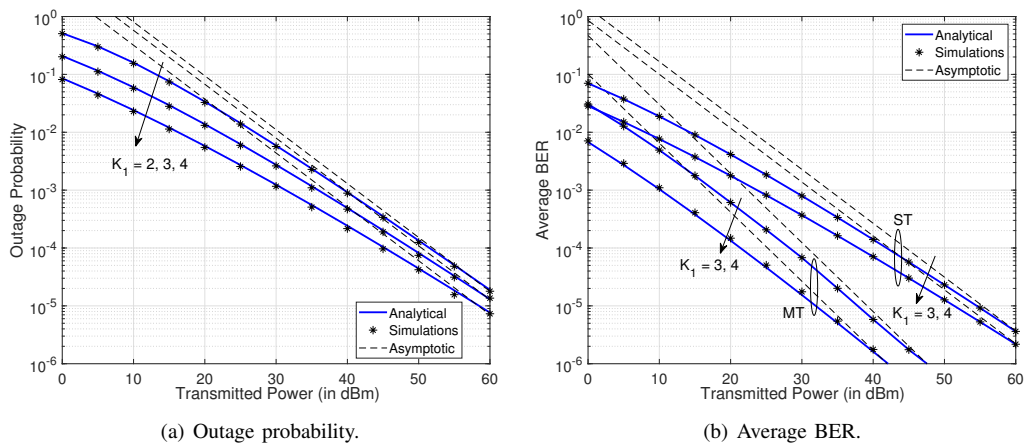


Fig. 3. Performance demonstration of multi-RIS transmissions for FSO link.

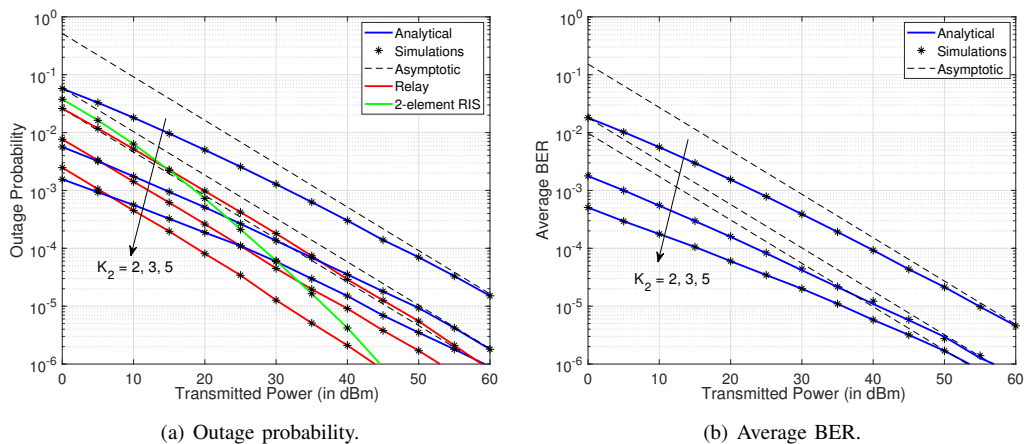


Fig. 4. Performance demonstration of multi-RIS transmissions for R2V link.

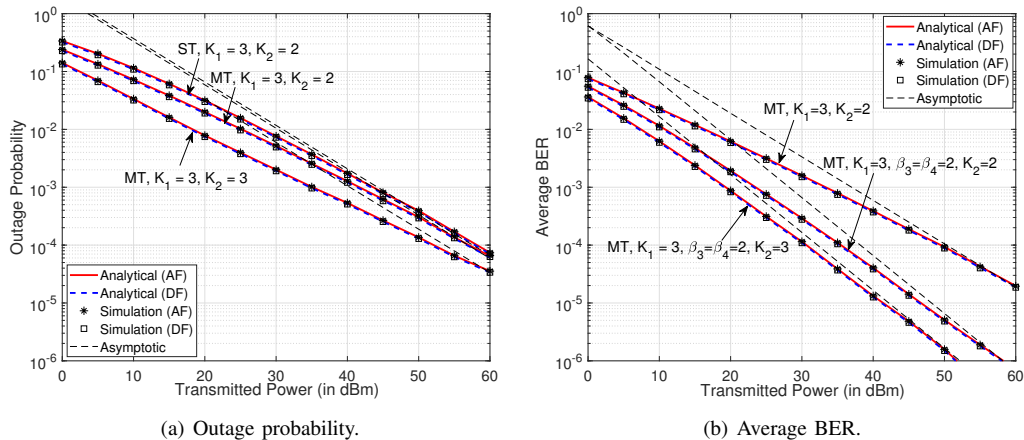


Fig. 5. Performance demonstration of RIS-assisted multi-hop mixed FSO-R2V system.

RISs for FSO (Fig. 3(a) and Fig. 3(b)) and RF transmissions (Fig. 4(a) and Fig. 4(b)). We plot the outage performance of FSO system for ST scenario and for different hops  $K_1 = 2, 3, 4$  in Fig. 3(a). It can be seen that an increase in the number of optical RIS modules between the source and relay increases the performance due to a decrease in the effect of pointing errors with close placement of RIS modules. In particular, with  $K_1 = 2$ , FSO links suffer from higher pointing errors  $\rho = 2.5$  but when the number of optical RIS modules are increased to 2 for  $K_1 = 3$ , FSO signal in each hop suffers from relatively lesser pointing error  $\rho = 5$ . Further, with  $K_1 = 4$  i.e., 3-optical RIS modules between source and relay, FSO transmissions have negligible or no pointing errors in each hop. Thus the multi-RIS deployment improves the FSO system performance with an increase in the number of hops or optical RIS modules. Moreover, lesser transmit power is needed with an increase in the optical RIS modules to achieve a desired performance. For example, for an outage performance of  $10^{-3}$ , we need 30dBm of transmit power with  $K_1 = 4$  but  $P_t = 35$ dBm and  $P_t = 40$ dBm for  $K_1 = 3$  and  $K_1 = 2$  hops respectively. The figure also depicts that the diversity order or the slope of the outage plots is the same for different  $K_1$ -hops as the diversity order is determined by the atmospheric turbulence parameters (ST) independent of pointing errors.

The average BER performance of multi-hop optical RIS FSO system is shown in Fig. 3(b) for ST and MT atmospheric turbulence scenarios with  $K_1 = 3, 4$ . Here, BER performance improves with an increase in the number of optical RIS modules due to negligible or no pointing error at higher  $K_1$ . It can be seen that strong turbulence requires an additional 15 dBm of the transmit power compared with the moderate scenario to achieve an outage probability of  $10^{-4}$  for  $K_1 = 3$  and 20 dBm for  $K_1 = 4$ . The plot also shows that the diversity depends on FSO system parameters as the average BER plots are steeper for MT (diversity order  $G_{\text{BER}} = 1.12$ ) when compared with ST scenario ( $G_{\text{BER}} = 0.93$ ).

Under the similar practical setup, we illustrate the outage probability Fig. 4(a) and the average BER performance Fig. 4(b) for multi-hop RF system. Here, we consider higher shadowing and also larger path loss exponent  $a$  for lower  $K_2$  and subsequently comparatively lesser parameters for higher  $K_2$  to depict the scenario of good channel conditions with an increase in RIS modules. The figure depicts that there is an

enhancement in the RF system performance with an increase in the number of RIS modules or hops. For a comparison, we have also plotted multi-hop DF relay performance in Fig. 4(a) using path loss exponent  $a = 4$  for all  $K_2$ . It can be seen that the DF relay performance is better than that of multi-hop RIS system requiring more energy consumption compared with the RIS-based system. We have also plotted a single RIS system with 2-elements (assuming perfect phase compensation) performing better at a high SNR. Note that we consider a single-element RIS since it is hard for phase compensation for multiple-element RIS in the multi-hop scenario. In Fig. 4(b), we have shown the average BER performance for different  $K_2$ . Here, the average BER performance improves with an increase in  $K_2$  due to reduced effect of shadowing and path loss. As  $K_2$  increases, we require a less transmit power to achieve the desired performance. For example, a transmit power of 10dBm is needed at  $K_2 = 3$  when compared with 25dBm at  $K_2 = 2$  to achieve a desired average BER performance of  $10^{-3}$ .

In Fig. 5(a) and 5(b), we demonstrate the impact of multiple RIS modules on the performance of a mixed FSO-RF system. We consider both ST and MT with  $K_1 = 3$  hops in the FSO links. We plot the outage probability as depicted in Fig. 5 (a) for both DF and AF relay by considering  $K_1 = 3$  hops in the FSO link and  $K_2 = 2, K_2 = 3$  RF links to demonstrate the improvement in performance with an increase in  $K_2$ . Finally in Fig. 5 (b), we simulate the average BER performance of mixed FSO-RF system with MT,  $K_1 = 3$  in FSO links and  $K_2 = 2, 3$  in RF links. We also vary the parameter  $\beta$  to depict that the diversity order of the system depending on fading parameters. It can be seen from the figure that an increase in the parameter  $\beta$  improves the performance due to the decrease in the fading severity.

Finally, we compare the average BER performance of our proposed system with other system configurations, as described in the caption of Fig. 6, for both equal and unequal placement of RIS modules. The results demonstrate that the placement of RIS modules in the equidistant (ED) and non-equidistant (NED) configurations (represented by the black and red plots, respectively) have negligible impact on the average BER performance of our multihop scheme. However, the unequal placement of RIS modules performs slightly better than the equidistant scenario due to lower path loss. This finding may motivate further investigation into optimizing

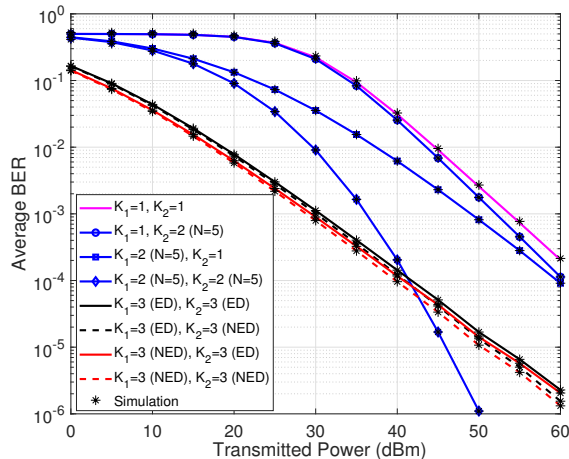


Fig. 6. Performance comparison of RIS-assisted multi-hop mixed FSO-RF system with other system configurations. Here,  $\{K_1 = 1, K_2 = 1\}$ : without FSO-RIS and without RF-RIS;  $\{K_1 = 1, K_2 = 2(N = 5)\}$ : without FSO-RIS and single RF-RIS with 5 elements;  $\{K_1 = 2(N = 5), K_2 = 1\}$ : single FSO-RIS with 5 elements and without RF-RIS;  $\{K_1 = 2(N = 5), K_2 = 2(N = 5)\}$ : single FSO-RIS with 5 elements and single RF-RIS with 5 elements;  $K_1 = 3$  and  $K_2 = 3$ : proposed multihop (i.e. 2 FSO-RIS with single element and 2 RF-RIS with single element); ED: equidistant placement of RISs; NED: non-equidistant placement of RISs;  $d_1 = 1000\text{m}$  and  $d_2 = 300\text{m}$ . NED for FSO has first RIS at 200m and second RIS at 500m, and NED for RF has first RIS at 40m and second RIS at 160m.

the placement distance to enhance performance further. We also demonstrate the average BER performance of single RIS modules containing five elements (illustrated by three blue-colored plots). The results show that incorporating RIS modules in FSO and RF links yields better performance than employing RIS solely in FSO or RF. The illustration indicates that the suggested multihop transmission approach (employing 2 RIS modules with one element each in FSO and RF connections) outperforms the single RIS module method (featuring five elements each in FSO and RF connections) for a usable transmission power of up to 40 dBm. Moreover, using RIS modules leads to improved outcomes compared to situations without RIS implementation, as demonstrated by the magenta plots.

## VII. CONCLUSIONS

We investigated the multiple RIS empowered mixed FSO-RF multihop system for vehicular communications. We developed a framework to derive PDF and CDF of cascaded channels for generalized fading models by considering single-element RIS avoiding complex procedure for phase compensation compared with the multiple-element RIS system under multi-hop scenario. We employed AF and DF relaying protocols to mix two different technologies and presented system performance by deriving analytical expressions for the outage probability and average BER. We also analyzed asymptotic behavior of the outage probability in the high SNR using Gamma functions to reveal insight on the effect of channel parameters on the system performance. Simulation results demonstrated the effectiveness of multiple RISs modules to achieve LOS propagation for FSO transmissions and reliable connectivity for vehicular communication. In FSO links, the use of multiple RIS modules reduces the pointing error in each hop due to perfect beam alignment with subsequent use of multiple RIS. With the multiple RF-RIS deployment,

the effect of deep shadowing can be reduced due to close proximity of RISs. The suggested multi-hop transmission approach may surpass the single RIS module technique in specific situations of practical importance. The suggested multiple RIS based communications can be a suitable candidate to provide seamless connectivity for autonomous vehicular systems. Although the relaying system performance is better, the RIS-based system is more energy efficient and requires less power consumption.

In the future, the proposed work could encompass a thorough, measurement-based channel analysis for multihop-based RIS systems to improve performance evaluation. Additionally, optimizing the positioning of RIS modules may present a feasible solution for boosting overall performance.

## APPENDIX A

Most of the works in the literature use induction based approach to compute the PDF of product of random variables. However, similar analysis cannot be used for all the generalized fading models. Thus, we employ Mellin's transform to compute the PDF of the product of random variables. The Mellin's transform of a function  $f_X(x)$  is given as [39]

$$M(r) = M\{f_X(x)\} = \int_0^\infty f_X(x)x^{-r} dx \quad (47)$$

The inverse Mellin's transform as

$$f_X(x) = \frac{1}{x} \frac{1}{2\pi j} \int_{\mathcal{L}} M(r)x^{-r} dr \quad (48)$$

If  $f_X(x)$  is the PDF then its Mellin's transform is nothing but the  $r^{\text{th}}$ -moment  $\mathbb{E}[X^r]$ . Thus, we use the Mellin's transform to find the PDF of the product of  $K$  random variables as [39]

$$f_X(x) = \frac{1}{x} \frac{1}{2\pi j} \int_{\mathcal{L}} \prod_{i=1}^K \mathbb{E}[X_i^r] x^{-r} dr \quad (49)$$

Substituting (20) in  $\mathbb{E}[X_i^n] = \int_0^\infty x^n f_{X_i}(x) dx$  and using the identity [37, eq. 2.8], the  $r$ -th moment can be computed as

$$\begin{aligned} \mathbb{E}[X_i^r] &= \psi_i \int_0^\infty x^{r+\phi_i-1} H_{p,q}^{m,n} \left[ \zeta_i x \mid \left\{ \begin{matrix} (a_{i,j}, A_{i,j}) \\ (b_{i,j}, B_{i,j}) \end{matrix} \right\}_{j=1}^p \right] dx \\ &= \psi_i \zeta_i^{-r-\phi_i} \frac{\prod_{j=1}^m \Gamma(b_{i,j} + B_{i,j}(r + \phi_i))}{\prod_{j=n+1}^p \Gamma(a_{i,j} + A_{i,j}(r + \phi_i))} \\ &\quad \frac{\prod_{j=1}^n \Gamma(1 - a_{i,j} - A_{i,j}(r + \phi_i))}{\prod_{j=m+1}^q \Gamma(1 - b_{i,j} - B_{i,j}(r + \phi_i))} \end{aligned} \quad (50)$$

We use (50) in (49) and apply the integral representation of the Fox's-H function to get (21). Using (21) in  $F_X(x) = \int_0^x f_X(t) dt$ , an expression for the CDF:

$$\begin{aligned} F_X(x) &= \prod_{i=1}^K \psi_i \zeta_i^{-\phi_i} \frac{1}{2\pi j} \int_{\mathcal{L}} \left( \prod_{i=1}^K \zeta_i \right)^r \left( \int_0^x t^{-1+r} dt \right) \\ &\quad \frac{\prod_{i=1}^K \prod_{j=1}^m \Gamma(b_{i,j} + B_{i,j}(-r + \phi_i))}{\prod_{i=1}^K \prod_{j=n+1}^p \Gamma(a_{i,j} + A_{i,j}(-r + \phi_i))} \\ &\quad \frac{\prod_{i=1}^K \prod_{j=1}^n \Gamma(1 - a_{i,j} - A_{i,j}(-r + \phi_i))}{\prod_{i=1}^K \prod_{j=m+1}^q \Gamma(1 - b_{i,j} - B_{i,j}(-r + \phi_i))} dr \end{aligned} \quad (51)$$

Using the inner integral  $\int_0^x t^{-1+r} dt = \frac{x^r}{r} = x^r \frac{\Gamma(r)}{\Gamma(1+r)}$  in (51), and applying the definition of Fox's-H function, we get (22), which concludes the proof.

## REFERENCES

- [1] V. K. Chapala and S. M. Zafaruddin, "Reconfigurable intelligent surface empowered multi-hop transmission over generalized fading," in *2022 IEEE 95th Veh. Tech. Conf.: (VTC2022-Spring)*, 2022, pp. 1–5.
- [2] M. D. Renzo *et al.*, "Smart radio environments empowered by reconfigurable AI meta-surfaces: An idea whose time has come," *EURASIP Journal on Wireless Communications Networking*, vol. 2019, no. 129, May 2019.
- [3] E. Basar *et al.*, "Wireless communications through reconfigurable intelligent surfaces," *IEEE Access*, vol. 7, pp. 116753–116773, Aug. 2019.
- [4] Q. Wu *et al.*, "Intelligent reflecting surface aided wireless communications: A tutorial," *IEEE Transactions on Communications*, vol. 69, no. 5, pp. 3313–3351, Jan. 2021.
- [5] Y. Zhu *et al.*, "Intelligent reflecting surface-aided vehicular networks toward 6G: Vision, proposal, and future directions," *IEEE Veh. Technol. Mag.*, vol. 16, no. 4, pp. 2–10, Dec. 2021.
- [6] A. Trichili *et al.*, "Roadmap to free space optics," *J. Opt. Soc. Am. B*, vol. 37, no. 11, pp. A184–A201, Nov 2020.
- [7] J. Wang *et al.*, "Outage analysis for intelligent reflecting surface assisted vehicular communication networks," [Online], arXiv: 2004.08063, 2020.
- [8] K. Odeyemi *et al.*, "Reconfigurable intelligent surface assisted mobile network with randomly moving user over Fisher-Snedecor fading channel," *Physical Communication*, vol. 43, p. 101186, Aug. 2020.
- [9] I. Trigui *et al.*, "A comprehensive study of reconfigurable intelligent surfaces in generalized fading," arXiv Preprint: 2004.02922, 2020.
- [10] H. Du *et al.*, "Millimeter wave communications with reconfigurable intelligent surfaces: Performance analysis and optimization," *IEEE Transactions on Communications*, vol. 69, no. 4, pp. 2752–2768, Jan. 2021.
- [11] V. Jamali *et al.*, "Intelligent reflecting surface assisted free-space optical communications," *IEEE Commun. Magazine*, vol. 59, no. 10, pp. 57–63, Nov. 2021.
- [12] M. Najafi and R. Schober, "Intelligent reflecting surfaces for free space optical communications," in *2019 IEEE Global Communication Conference (GC'09)*, USA, Dec. 2019, pp. 1–7.
- [13] A. R. Ndjiongue *et al.*, "Performance analysis of RIS-based nT-FSO link over  $G$ - $G$  turbulence with pointing errors," arXiv Preprint: 2102.03654, 2021.
- [14] V. K. Chapala and S. M. Zafaruddin, "Unified performance analysis of reconfigurable intelligent surface empowered free space optical communications," *IEEE Transactions on Communications*, vol. 70, no. 4, pp. 2575–2592, April 2022.
- [15] H. Du *et al.*, "Performance and optimization of reconfigurable intelligent surface aided THz communications," *IEEE Transactions on Communications*, vol. 70, no. 5, pp. 3575–3593, 2022.
- [16] K. Dovelos *et al.*, "Intelligent reflecting surfaces at terahertz bands: channel modeling and analysis," [Online], arXiv: 2103.15239, 2021.
- [17] V. K. Chapala and S. M. Zafaruddin, "Exact Analysis of RIS-Aided THz Wireless Systems Over  $\alpha$ - $\mu$  Fading with Pointing Errors," *IEEE Commun. Lett.*, vol. 25, no. 11, pp. 3508–3512, Nov. 2021.
- [18] Y. U. Ozcan *et al.*, "Reconfigurable intelligent surfaces for the connectivity of autonomous vehicles," *IEEE Trans. Vehi. Technol.*, vol. 70, no. 3, pp. 2508–2513, March 2021.
- [19] C. Huang *et al.*, "Multi-hop RIS-empowered terahertz communications: A DRL-based hybrid beamforming design," *IEEE J. Sel. Areas Commun.*, vol. 39, no. 6, pp. 1663–1677, June 2021.
- [20] A.-A. A. Boulgeorgos, N. Chatzidiamantis, H. G. Sandalidis, A. Alexiou, and M. D. Renzo, "Cascaded composite turbulence and misalignment: Statistical characterization and applications to reconfigurable intelligent surface-empowered wireless systems," *IEEE Trans. Vehi. Technol.*, pp. 1–1, 2022.
- [21] M. A. Kashani *et al.*, "A novel statistical channel model for turbulence-induced fading in free-space optical systems," *Journal of Lightwave Technology*, vol. 33, no. 11, pp. 2303–2312, June 2015.
- [22] H. AlQuwaiee *et al.*, "On the performance of free-space optical communication systems over double Generalized Gamma channel," *IEEE J. Sel. Areas Commun.*, vol. 33, no. 9, pp. 1829–1840, Sept. 2015.
- [23] B. Ashrafzadeh *et al.*, "Unified performance analysis of multi-hop FSO systems over double generalized gamma turbulence channels with pointing errors," *IEEE Trans. Wirel. Commun.*, vol. 19, no. 11, pp. 7732–7746, Nov. 2020.
- [24] Z. Rahman *et al.*, "Performance of dual-hop relaying for OWC system over foggy channel with pointing errors and atmospheric turbulence," *IEEE Trans. Vehi. Technol.*, pp. 1–1, Dec. 2021.
- [25] P. S. Bithas *et al.*, "On the double-generalized gamma statistics and their application to the performance analysis of V2V communications," *IEEE Trans. Commun.*, vol. 66, no. 1, pp. 448–460, Jan. 2018.
- [26] L. Yang *et al.*, "Mixed dual-hop FSO-RF communication systems through reconfigurable intelligent surface," *IEEE Commun. Lett.*, vol. 24, no. 7, pp. 1558–1562, April 2020.
- [27] A. Sikri *et al.*, "Reconfigurable intelligent surface for mixed FSO-RF systems with co-channel interference," *IEEE Commun. Lett.*, vol. 25, no. 5, pp. 1605–1609, Feb. 2021.
- [28] A. M. Salhab and L. Yang, "Mixed RF/FSO relay networks: Ris-equipped rf source vs ris-aided rf source," *IEEE Wireless Communications Letters*, vol. 10, no. 8, pp. 1712–1716, Aug. 2021.
- [29] L. Yang *et al.*, "Indoor mixed dual-hop VLC/RF systems through reconfigurable intelligent surfaces," *IEEE Wireless Communications Letters*, vol. 9, no. 11, pp. 1995–1999, July 2020.
- [30] M. Hasna and M.-S. Alouini, "A performance study of dual-hop transmissions with fixed gain relays," *IEEE Trans. Wireless Commun.*, vol. 3, no. 6, pp. 1963–1968, Hong Kong, China, April 2004.
- [31] T. N. Do *et al.*, "Multi-ris-aided wireless systems: Statistical characterization and performance analysis," [Online], arXiv:2104.01912, Sept. 2021.
- [32] H. Wang *et al.*, "Performance of wireless optical communication with reconfigurable intelligent surfaces and random obstacles," arXiv preprint:2001.05715, 2020.
- [33] K.-J. Jung *et al.*, "Unified finite series approximation of FSO performance over strong turbulence combined with various pointing error conditions," *IEEE Transactions on Communications*, vol. 68, no. 10, pp. 6413–6425, Oct. 2020.
- [34] P. Ramirez-Espinosa and F. J. Lopez-Martinez, "Composite fading models based on inverse gamma shadowing: Theory and validation," *IEEE Trans. Wirel. Commun.*, vol. 20, no. 8, pp. 5034–5045, 2021.
- [35] K. Govindan, K. Zeng, and P. Mohapatra, "Probability density of the received power in mobile networks," *IEEE Transactions on Wireless Communications*, vol. 10, no. 11, pp. 3613–3619, 2011.
- [36] *The Wolfram function Site*, Accessed November 2022: <https://functions.wolfram.com/>.
- [37] A. Mathai *et al.*, *The H-Function: Theory and Applications*. Springer New York, 2009.
- [38] I. Gradshteyn *et al.*, *Table of Integrals, Series, And Products*, Jan. 2007.
- [39] A. Kilbas *et al.*, *H-Transforms: Theory and Applications*. CRC Press., Mar. 2004.
- [40] I. S. Ansari *et al.*, "A new formula for the BER of binary modulations with dual-branch selection over generalized-K composite fading channels," *IEEE Transactions on Communications*, vol. 59, no. 10, pp. 2654–2658, Oct. 2011.
- [41] T. A. Tsiftsis *et al.*, "Multihop free-space optical communications over strong turbulence channels," in *2006 IEEE Int. Conf. on Commun.*, vol. 6, Istanbul, Turkey, June 2006, pp. 2755–2759.
- [42] I. I. Kim *et al.*, "Comparison of laser beam propagation at 785 nm and 1550 nm in fog and haze for optical wireless communications," *Proc. SPIE*, vol. 4214, pp. 26–37, Nov. 2001.
- [43] W. Tang *et al.*, "Wireless communications with reconfigurable intelligent surface: Path loss modeling and experimental measurement," *IEEE Trans. Wireless Commun.*, vol. 20, no. 1, pp. 421–439, Jan 2021.